Journal of Hazardous Materials 465 (2024) 133298

Contents lists available at ScienceDirect

Journal of Hazardous Materials

journal homepage: www.elsevier.com/locate/jhazmat

Research Paper

Differential response of Hg-methylating and MeHg-demethylating microbiomes to dissolved organic matter components in eutrophic lake water

Zhengyu Wu [a], Zhike Li [a], Bo Shao [a], Ji Chen [b], Xiaomei Cui [c], Xiaoyu Cui [a], Xianhua Liu [a], Ying Xin Zhao [a], Qiang Pu [b], Jiang Liu [b], Wei He [d], Yiwen Liu [a], Yurong Liu [e], Xuejun Wang [f], Bo Meng [b,*], Yindong Tong [a,c,**]

[a] School of Environmental Science and Engineering, Tianjin University, Tianjin 300072, China
[b] State Key Laboratory of Environmental Geochemistry, Institute of Geochemistry, Chinese Academy of Sciences, Guiyang 550081, China
[c] School of Ecology and Environment, Tibet University, Lhasa 850000, China
[d] School of Water Resource and Environment, China University of Geoscience (Beijing), Beijing 100083, China
[e] State Key Laboratory of Agricultural Microbiology, Huazhong Agricultural University, Wuhan 430070, China
[f] College of Urban and Environmental Sciences, Peking University, Beijing 100871, China

HIGHLIGHTS

- AOM boosted methylation rate constants by 1−2 orders of magnitude compared to TOM.
- Hg methylators and MeHg demethylators responded differently to DOM treatments.
- Hg methylation and associated microbes correlated with specific DOM components.

GRAPHICAL ABSTRACT

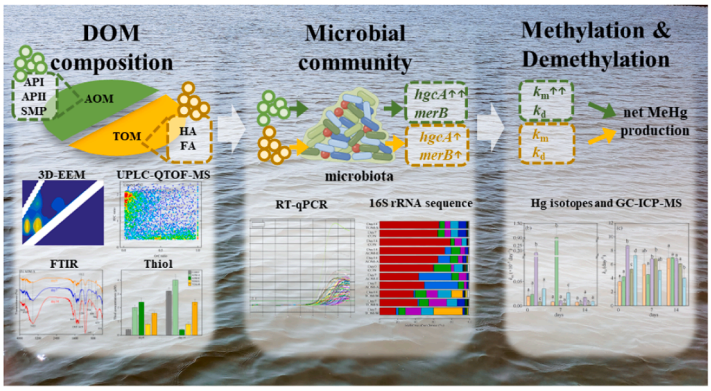

ARTICLE INFO

Editor: Lingxin CHEN

Keywords:
Dissolved organic matter
Net MeHg production
Hg methylation

ABSTRACT

Methylmercury (MeHg) production in aquatic ecosystems is a global concern because of its neurotoxic effect. Dissolved organic matter (DOM) plays a crucial role in biogeochemical cycling of Hg. However, owing to its complex composition, the effects of DOM on net MeHg production have not been fully understood. Here, the Hg isotope tracer technique combined with different DOM treatments was employed to explore the influences of DOM with divergent compositions on Hg methylation/demethylation and its microbial mechanisms in eutrophic lake waters. Our results showed that algae-derived DOM treatments enhanced MeHg concentrations by

* Correspondence to: Institute of Geochemistry, CAS, China.
** Corresponding author at: School of Environmental Science and Engineering, Tianjin University, Tianjin 300072, China.
E-mail addresses: mengbo@vip.skleg.cn (B. Meng), yindongtong@tju.edu.cn (Y. Tong).

https://doi.org/10.1016/j.jhazmat.2023.133298
Received 14 September 2023; Received in revised form 1 December 2023; Accepted 15 December 2023
Available online 18 December 2023

MeHg demethylation
Hg isotope tracer

1.42−1.53 times compared with terrestrial-derived DOM. Algae-derived DOM had largely increased the methylation rate constants by approximately 1−2 orders of magnitude compared to terrestrial-derived DOM, but its effects on demethylation rate constants were less pronounced, resulting in the enhancement of net MeHg formation. The abundance of *hgcA* and *merB* genes suggested that Hg-methylating and MeHg-demethylating microbiomes responded differently to DOM treatments. Specific DOM components (e.g., aromatic proteins and soluble microbial byproducts) were positively correlated with both methylation rate constants and the abundance of Hg-methylating microbiomes. Our results highlight that the DOM composition influences the Hg methylation and MeHg demethylation differently and should be incorporated into future Hg risk assessments in aquatic ecosystems.

1. Introduction

Mercury (Hg) has been well recognized as a priority pollutant, particularly due to its highly neurotoxic and organic form methylmercury (MeHg) [46,4,57]. MeHg has the potential to undergo significant biomagnification in aquatic food chains, which could ultimately pose a threat to organisms, including the humans [24,67,68]. Most Hg inputs from anthropogenic activities exist in an inorganic form that could be methylated to MeHg under typical conditions [44,6]. Anaerobic microbial inorganic Hg methylation is generally considered the predominant pathway for MeHg production in the aquatic environment [17,20,76]. This process is closely related to one-carbon metabolism and is regulated by the Hg methylator (e.g., sulfate-reducing bacteria, iron-reducing bacteria, and methanogens) carrying *hgcAB* genes [52]. In contrast, MeHg could be demethylated via the biotic reduction, biotic oxidation, and abiotic chemical demethylation pathways [3]. The observed MeHg concentration in the natural environment is a result of both Hg methylation and demethylation processes [3,35,37]. Previous studies have indicated that lakes can be hot spots for MeHg production [14,18,55], and the co-occurrences of Hg pollutions and eutrophication in lakes have been observed [71].

MeHg production in the aquatic environments is influenced by a combination of physical, chemical, and biological factors, including microbial taxon abundance and community structure, Hg(II) speciation and concentrations, dissolved organic matter (DOM), redox potentials, water temperatures, and pH [44,47,69]. DOM is well recognized as one of the most important drivers in determining MeHg productions. As the human activities intensify, DOM inputs from autochthonous and allochthonous sources are increasingly entering lake waters [79,83], making it crucial to understand the processes that determine MeHg production in these environments. DOM can act as a chemical ligand for both Hg(II) and MeHg [27], and serve as a growth substrate for microbes [61]. The dual role of DOM strongly affects speciation and bioavailability of Hg and, subsequently, productions and accumulations of MeHg in aquatic environments [45,59,80]. Previous studies have demonstrated that DOM plays important but complicated roles in Hg methylation, which has been demonstrated to promote or inhibit Hg methylation [29,48,50,54]. The sources of DOM and its composition in aquatic ecosystems are complex. The mechanism by which DOM of different compositions can regulates microbial Hg methylation or demethylation processes remains elusive.

DOM is a heterogeneous mixture of allochthonous or autochthonous sources, including small molecular compounds (e.g., monosaccharides, amino acids) and macromolecules (e.g., proteins, polysaccharides, lignin, and humus) [16,25,31]. Eutrophication and intensified anthropogenic alterations in both terrestrial and inland aquatic ecosystems have significantly increased nutrient and DOM inputs into the receiving ecosystems [82]. Algae-derived DOM (AOM) has received increasing attentions owing to its potential influence on microbial communities and contaminant transformations [2,7,70]. However, impacts of both AOM and terrestrial organic matter (TOM) on MeHg production remain debated and controversial. Phytoplankton-derived organic compounds have been found to stimulate Hg methylation in boreal lakes; however, this phenomenon has not been observed in water dominated by TOM [5]. Thus, it is necessary to characterize compositions of DOM from different sources and investigate their effect on MeHg production. In addition, many studies have focused mainly on changes in MeHg concentration, whereas underlying biotic methylation or demethylation process and responses of microbial communities remain poorly understood.

In this study, we applied the stable Hg isotope tracer techniques together with different DOM treatments to reveal effects of DOM compositions on Hg methylation and MeHg demethylation process. Specific Hg isotope tracers including $^{202}Hg^{II}$ and $Me^{198}Hg$, real-time quantitative PCR (qPCR) for the *hgcA/merB* genes, and 16S rRNA gene sequencing were combined to reveal Hg methylation/demethylation rates and understand the microbial mechanisms. DOM composition was characterized using the ultra-high-performance liquid chromatography-time-of-flight mass spectrometry (UPLC-QTOF-MS) and three-dimensional excitation-emission matrix (3D-EEM) fluorescence spectroscopy. The objectives of this study were (I) to investigate Hg methylation and MeHg demethylation processes in lake waters under different DOM treatments and (II) to assess the influence of DOM compositions on net MeHg productions and the abundance of Hg methylators/demethylators. Results of this study improve our understanding of the exact roles of the DOM composition in determining MeHg production in aquatic ecosystems.

2. Materials and methods

2.1. Preparations of DOM from different sources

Four typical DOM with different sources had been prepared for the incubation experiments, including two AOM from freshwater phytoplankton species (i.e., *Microcystis aeruginosa* and *Microcystis elabens*) and two TOM from the shrub soil (E: 117°20'02.44'', N: 38°59'50.23'') and wetland soil (E: 117°20'09.13'', N: 38°59'45.07'') (Fig. S1). Two algal species, *M. aeruginosa* and *M. elabens* were obtained from the Freshwater Algae Culture Collection of the Institute of Hydrobiology, China (Fig. S2). It should be noted that the selected algae are ubiquitously distributed in freshwater lakes and are often responsible for algal blooms [13,63]. AOM was extracted from the algae using a freeze-thaw method [12,35,37], and TOM was extracted from the soils using water extraction method [28]. Details of the DOM extractions are provided in Text S1.

2.2. Incubation experimental design

Two incubation experiments were designed to investigate the influences of different DOM treatments on MeHg production and the underlying mechanisms in water from a eutrophic lake (Fig. 1 and Table S1). Four sources of DOM were added to lake waters for further incubation for as long as 14 d, including AOM derived from *M. aeruginosa* (AOM-A) and *M. elabens* (AOM-E), and TOM derived from shrub soil (TOM-S) and wetland soil (TOM-W). As shown in Fig. 1, Experiment 1 aimed to investigate changes in net MeHg production under different DOM treatments. Experiment 2 was designed to trace the detailed changes in Hg methylation/demethylation rate constants, specific marker genes involved in methylation and demethylation processes

(i.e., *hgcA* and *merB*), and microbial communities with different DOM treatments.

Haijiao Lake (E: 117°20′02.44″, N: 38°59′50.23″) is characterized by a eutrophic status. It is located in the city of Tianjin, with a surface area of 1.07 km^2 and a history of *M. aeruginosa* blooms in the summer and autumn. Water samples were collected from this lake on April 15th, 2022, prior to the algal blooms. Approximately 30 L of unfiltered surface water (1–50 cm) was collected in precleaned borosilicate glass bottle, transferred to the laboratory, and stored at 4 °C in the dark for the further incubations. The total Hg (5.11 ± 0.59 ng L^{-1}) and MeHg (0.38 ± 0.07 ng L^{-1}) concentrations in the unfiltered water sample were measured according to the EPA 1631 and 1630 methods (n = 3). The corresponding total nitrogen, total phosphorus, chlorophyll-a, and dissolved organic carbon (DOC) concentrations are listed in Table S2.

For the Experiment 1, five treatments (i.e., AOM-A, AOM-E, TOM-S, TOM-W, and control) were prepared. Unfiltered lake water (90 mL), DOM solution, and the standard $HgCl_2$ solution (Aladdin, China) were mixed in the pre-cleaned 150 mL borosilicate glass bottle in an oxygen free glove box (PLAS-LABS, USA; 90% Ar + 10% H_2), and the final volume was adjusted to 120 mL using ultrapure water. The added concentration of DOM was set to 10 mg C L^{-1}, based on the ambient DOM concentration in the lake water sample. In addition, Hg was spiked at an Hg:C ratio of 1:20,000 to ensure accurate measurements of in situ MeHg production [33,75]. The glass bottles were tightly sealed using butyl rubber and screw caps, blended, and then incubated at approximately 25 °C in the dark. Each treatment was performed in triplicate. Three random replicates for each treatment were collected at 0, 1, 7, and 14 days. The mixtures were filtered through a 0.22-μm PTFE membrane (Millipore®, USA), acidified to 0.4% (*v/v*) using concentrated hydrochloric acid (HCl), and stored at 4 °C in the dark for the MeHg analysis.

Experiment 2 was designed to characterize methylation of inorganic Hg and demethylation of MeHg during incubation. The DOM composition, the abundance of the Hg methylation gene (*hgcA*) and MeHg demethylation gene (*merB*), and changes in the microbial communities were also investigated. Similar to Experiment 1, five treatments were conducted in an oxygen-free glove box: AOM-A, AOM-E, TOM-S, TOM-W, and one control. The incubation samples were subjected to the same treatment as in Experiment 1, which involved the uses of unfiltered lake waters and DOM addition. To trace specific Hg methylation and demethylation at various time points during the incubations (i.e., 0, 7, and 14 d), samples with different DOM treatments were incubated for 0, 7, and 14 d. At these time intervals, the Hg isotope tracers (i.e., $^{202}Hg^{II}$ and $Me^{198}Hg$) were spiked into the sample for an additional 12 h of incubation, with a final concentration of 5 ng L^{-1}, adjusted according to the ambient Hg concentration in lake water [41,39,73]. After this, 20 mL incubated water was transferred to borosilicate glass tubes, acidified to 0.4% (*v/v*) using concentrated HCl, and stored in the dark at approximately 4 °C until isotopic MeHg analysis. It should be noted that the rate constant on day 0 represented the mean rate of 12 h on day 0, rather than the initial rate. Remaining water sample was filtered through 0.22-μm polycarbonate membranes (Millipore, USA). The membranes were frozen at − 80 °C for the microbiological analyses, and the filtrate was stored at − 20 °C for the DOM characterizations.

2.3. MeHg concentration analysis

MeHg concentration was determined using gas chromatography coupled with cold vapor atomic fluorescence spectrometry (CVAFS, Tekran 2500) according to the EPA method 1630. In summary, 25 mL of water sample and 0.1 mL of saturated $CuSO_4$ were transferred into a 50-mL Teflon vial, followed by distillation at ~125 °C for 2 h. The distillate was collected in a 40-mL glass vial, containing 4.5 mL of distilled water and 0.5 mL of 2 M acetate buffer. All glass vials were kept at a temperature of approximately 5 °C to avoid the losses of MeHg. The MeHg in the distillate was ethylated with sodium tetraethylborate, purged, and captured on a Tenax adsorbent column. The ethylated Hg species were thermally desorbed to gas chromatography and detected using CVAFS. The method detection limit (3σ) was 0.046 ng L^{-1} for MeHg in the water samples. The variability between triplicate samples was less than 8.9%, and the recovery of matrix spikes in the water samples ranged from 81% to 110%.

MeHg isotopes were analyzed using a gas chromatography-inductively coupled plasma-mass spectrometry system (Agilent 7700x) following the distillation-ethylation-purge-trap method [35,37,61]. Hg isotopes, including $Me^{198}Hg^+$ (demethylation tracer), $Me^{199}Hg^+$, $Me^{200}Hg^+$, $Me^{201}Hg^+$, and $Me^{202}Hg^+$ (methylation tracer), have been

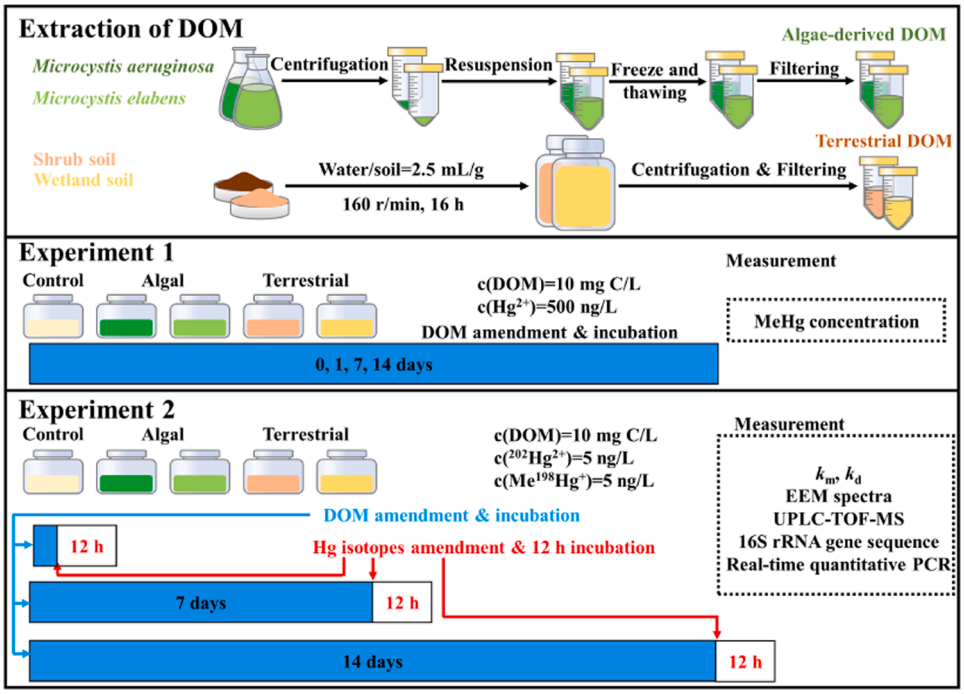

Fig. 1. A diagram showing the preparation of different DOM treatments and two incubation experiments with DOM treatments from different sources.

studied [41,39,38]. Isotope-enriched inorganic Hg tracers ($^{202}Hg^{II}$) and MeHg tracers ($Me^{198}Hg^{+}$) were used to trace the rates of inorganic Hg methylation and MeHg demethylation, respectively. $^{202}Hg(NO_3)_2$ was prepared by dissolving $^{202}Hg^0$ (98.68 ± 0.2% purity; ISOFLEX, USA) in nitric acid (≥ 99.9%, trace metal basis), and the $Me^{198}HgNO_3$ was prepared using a methylcobalamin method with $^{198}Hg(NO_3)_2$ (98.52 ± 0.15% purity; ISOFLEX, USA) following previous studies [40,58]. In addition, an external MeHg standard (Brooks Rand, USA) was applied to quantify the ambient and Hg tracer concentrations. The methylation rate constant (k_m) and demethylation rate constant (k_d) were calculated from increases in $Me^{202}Hg^{+}$ and decreases in $Me^{198}Hg^{+}$ (n = 45) according to the irreversible pseudo-first-order rate law using Eqs. (1) and (2) [19,26,74]:

$$k_m = \frac{[Me^{202}Hg^{+}]_{t1} - [Me^{202}Hg^{+}]_{t0}}{[^{202}Hg^{II}] \times t} \quad (1)$$

$$k_d = \frac{\ln([Me^{198}Hg^{+}]_{t0}) - \ln([Me^{198}Hg^{+}]_{t1})}{t} \quad (2)$$

where $[Me^{202}Hg^{+}]_{t0}$ and $[Me^{198}Hg^{+}]_{t0}$ represent the isotopically enriched $Me^{202}Hg^{+}$ and $Me^{198}Hg^{+}$ concentrations at the initial time point (t_0), respectively; $[Me^{202}Hg^{+}]_{t1}$ and $[Me^{198}Hg^{+}]_{t1}$ are the $Me^{202}Hg^{+}$ and $Me^{198}Hg^{+}$ concentrations in the samples after 12-h incubations, respectively; $[^{202}Hg^{II}]$ represents the concentration of $^{202}Hg^{II}$ added to the samples as a spike; and t represents the incubation time after spiking with the isotopes.

Quality controls and assurance measurements had been implemented, including triplicates, method detection limits, field blanks, and matrix spike recoveries for all analytes. No significant MeHg contamination was detected in the blank samples. The method detection limit (3σ) for MeHg isotopes in the water samples was determined to be 0.013 ng L^{-1}. The variability between the triplicate samples was less than 9.3%, and the recoveries for MeHg isotope analyses in the water samples ranged from 75% to 114% for the matrix spikes.

2.4. DOM characterization and microbiological analysis

A combination of chemical analysis techniques, including EEM spectroscopy and UPLC-QTOF-MS, was used to characterize changes in DOM composition during incubation. Samples from the Experiment 2 were analyzed on days 0, 7, and 14 using a Hitachi F-7100 fluorometer. The emission spectral range was 250–600 nm, and excitation spectral range was 220–450 nm, both with steps of 5 nm. Fluorescence regional integration (FRI) was conducted on the dataset using a MATLAB toolbox DOMFluor [66,8]. Five DOM components were extracted from the spectral data: aromatic protein I (API), aromatic protein II (APII), and fulvic acid-like (FA), soluble microbial product-like (SMP) and humic acid-like (HA) materials. Details of the EEM measurements and FRI analysis are provided in Text S2. The thiol concentrations of samples were determined using the 5,5′-dithiobis-(2-nitrobenzoic acid) method [1,15]. The major functional groups of DOM were characterized using the Fourier-transform infrared spectroscopy (FTIR) (IRAffinity-1S, Shimadzu, Japan). The samples were freeze-dried at − 50 °C and stored in a dryer before testing. Spectroscopically pure potassium bromide was used for the tablet pressing. The displayed result was a single-averaged spectrum of 16 scans at a frequency of 4 cm^{-1}, analyzed in a range of 4000–400 cm^{-1} [35,37].

UPLC-QTOF-MS has been extensively used for autochthonous and allochthonous DOM in previous studies [53,36]. In this study, UPLC-QTOF-MS (Agilent /Brooke) was used to characterize molecular compositions [i.e., numbers, formulae, and charge mass ratio (m/z)] for four selected DOM sources. Details for pre-treatments and measurements are provided in Text S3. An in-house Matlab routine was applied to assign the formulas up to $C_{40}H_{80}O_{40}N_2S$ with or without one ^{13}C [25], and only the peaks with a signal/noise ≥ 10 were assigned. The error between the measured and calculated masses for a given chemical formula was < 5 ppm. These formulas must follow specific rules, including O/C < 1, H/C 0.3–2, m/z 100–1000, a non-negative integral double bond equivalent, and the nitrogen rule [30]. The assigned molecular formulae were predominantly composed of carbon, hydrogen, and oxygen (CHO), followed by formulae with additional nitrogen (CHON), sulfur (CHOS) or both nitrogen and sulfur (CHONS) [25].

Water samples from Experiment 2 on days 0, 7, and 14 were filtered through a sterilized 0.22-μm polycarbonate filter, after which they were used for the DNA extraction and bacterial community analysis by Sangon BioTech, China. Bacterial community compositions had been characterized using the Illumina MiSeq platform of the V3-V4 region of the 16S rRNA gene, amplified using primers 341 F/805 R (see the detail in Text S4). After sequencing, readings were assembled with PEAR (version 0.9.8), and the effective tags were clustered into the operational taxonomic units of ≥ 97% similarity [65]. To investigate change in methylators and demethylators during incubation, we adopted the method of Wang et al. [72] to define putative methylators and demethylators according to whether they carried the methylation gene *hgcA* and demethylation gene *merB*, as inferred from prior studies (Table S3). A co-occurrence network was established to identify associations between the microbial taxa (at the family level), including putative Hg methylators, MeHg demethylators, and other taxa. These networks were based on significant and strong correlations between microbial taxa (pairwise Spearman's rank correlation, $|\rho| > 0.50$ and $P < 0.01$), and the network was visualized using interactive platform Gephi.

Real-time quantitative PCR analysis was performed using the filtered membranes from the Experiment 2 on the days 0, 7, and 14. The abundance of the 16S rRNA, *hgcA*, and *merB* genes was quantified using reported primer pairs for the whole bacteria, methylators, or demethylators [10,49,60]. More details are provided in Text S4.

2.5. Statistical analysis

Data normality was assessed using the Shapiro-Wilk test in SPSS (version 22.0; IBM, USA). One-way analysis of variance (ANOVA) with Tukey's multiple comparison test was applied to compare statistical significance among treatments, and the Pearson's correlation analysis was conducted to explore relationships between different variables. A Mantel test using R software (V 4.0.2) [56] was conducted to examine the correlations between microbial community compositions and the DOM components.

3. Results

3.1. Effects of different DOM treatments on net MeHg production

In Experiment 1, we compared the changes of MeHg concentrations in lake waters with the four sources of DOM (Fig. 2). In general, the mean MeHg concentrations during the days 1–14 of incubations were 6.62 ± 3.97 ng L^{-1} for AOM-A, 6.12 ± 3.56 ng L^{-1} for AOM-E, 4.04 ± 2.06 ng L^{-1} for TOM-S, 4.01 ± 2.24 ng L^{-1} for TOM-W, and 3.71 ± 1.96 ng L^{-1} for the control groups (n = 3 for all treatments). Compared with the control treatments, the AOM-A and AOM-E treatments resulted in the MeHg concentrations for 131%−209% and 126.67%−185.15% ($P < 0.05$), respectively. Throughout the incubation period, the highest MeHg concentration was observed on day 7 for all the treatments. The AOM-A treatment showed the highest MeHg level, reaching up to 13.45 ± 2.90 ng L^{-1}. Furthermore, MeHg concentrations in the AOM treatments (AOM-A and AOM-E) were significantly higher than those in the TOM treatments (i.e., TOM-S and TOM-W) ($P < 0.05$). The trend in the MeHg concentrations varied among different DOM treatments during the incubations. For the TOM treatments, MeHg concentrations had initially increased and then remained stable over time. In contrast, MeHg concentrations in the control and AOM

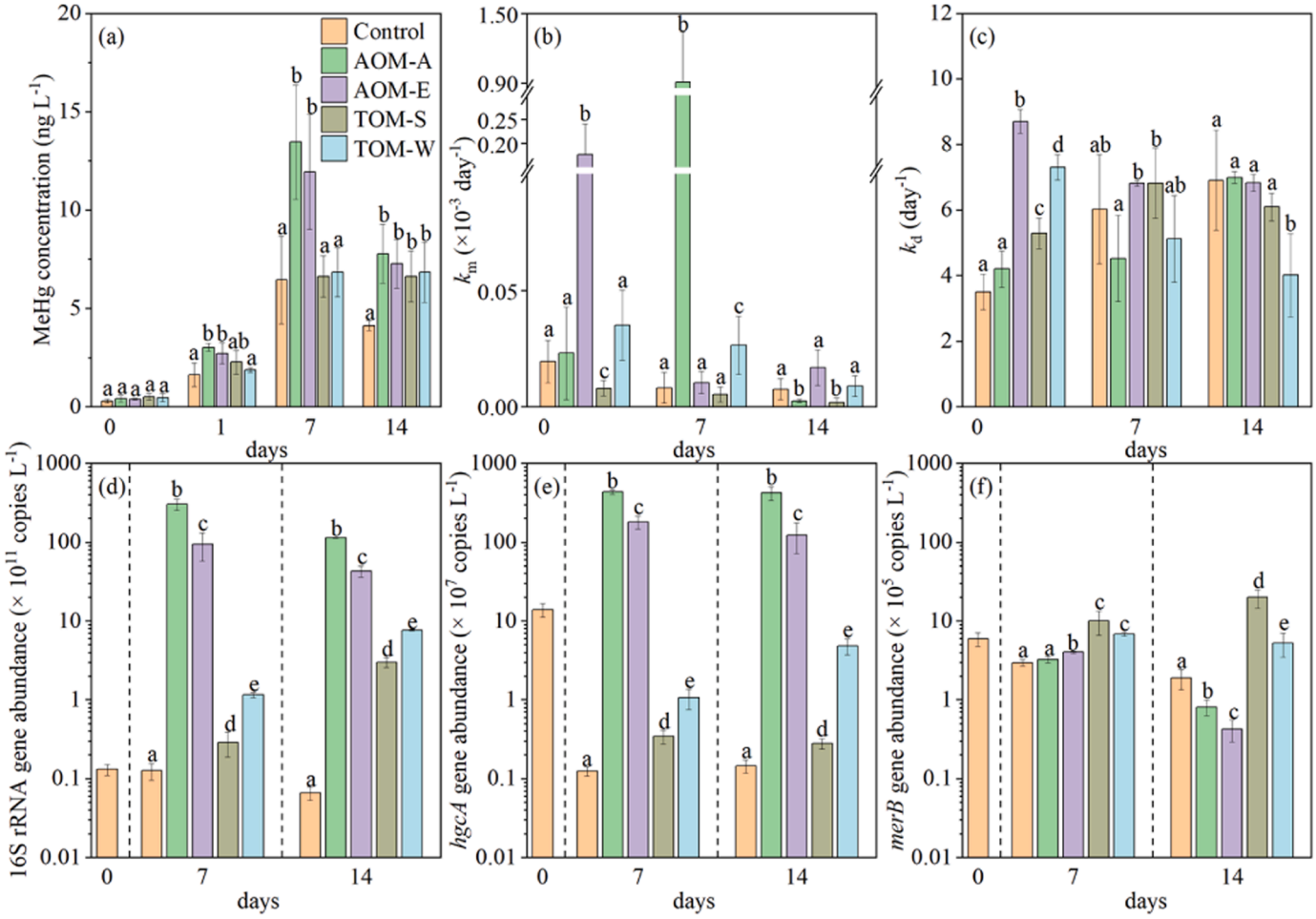

Fig. 2. Changes in MeHg concentrations during incubation with different DOM treatments in Experiment 1 (a); changes in the methylation and demethylation rate constants (b, c) and abundance of 16S rRNA gene (d), *hgcA* gene (e), and *merB* gene (f) during the incubation with different DOM treatments in the Experiment 2. The different lowercase letters above columns indicate significant differences ($P < 0.05$).

treatments initially increased but gradually decreased with extended incubation time. The decrease in the MeHg concentration at a later stage of incubation could be attributed to the change in the dominant process from Hg methylation to MeHg demethylation over time [33,41,39]. Fig. S3 illustrates the MeHg concentrations normalized by DOC concentrations, providing a representation of MeHg production at equivalent DOC quantities but with different compositions. After 14-day incubations, the normalized MeHg concentrations in the AOM groups were significantly higher than those in the control and TOM groups ($P < 0.05$, Fig. S3).

3.2. Effects of DOM treatments on Hg methylation and demethylation

The multi-compound-specific isotope labeling technique (i.e., $^{202}Hg^{II}$ and $Me^{198}Hg$) provided a more comprehensive explanation for change of net MeHg production observed in Experiment 1. Specifically, changes in the MeHg concentration could be attributed to alterations in the Hg methylation rate constants k_m and MeHg demethylation rate constants k_d (Fig. 2b and 2c). On day 0, the AOM-E treatment exhibited the highest k_m value (i.e., $1.77 \pm 0.64 \times 10^{-4}$ d^{-1}) that was significantly higher than those of the remaining treatments ($P < 0.05$). On day 7, the AOM-A treatment yielded the highest k_m value (i.e., $8.57 \pm 4.71 \times 10^{-4}$ d^{-1}), while k_m in the AOM-E treatment decreased to $1.04 \pm 0.47 \times 10^{-5}$ d^{-1}. On day 14, k_m remained at relatively low levels for all treatments, ranging from $0.19 - 1.67 \times 10^{-5}$ d^{-1}. Significant increases in k_m were observed in the AOM treatments (AOM-A and AOM-E). However, no discernible differences in k_m were observed between the TOM and control treatments ($P > 0.05$). Differently, k_d ranged from 3.50 to 8.69 d^{-1} regardless of the DOM sources during the incubation, and remained relatively stable compared to the k_m. Notably, the effect of DOM on MeHg demethylation was more pronounced initially. For example, on day 0, the k_d values in the AOM-E, TOM-S, and TOM-W treatments were significantly higher than those in the controls ($P < 0.05$). On days 7 and 14, there were no discernible difference in k_d values among the control, AOM-A, AOM-E, and TOM-S treatments ($P > 0.05$).

3.3. Microbes related to Hg methylation and MeHg demethylation

To investigate the influence of different DOM treatments on the microbial communities, we analyzed the compositions of the dominant microbes and putative Hg methylators (Fig. S4). Across all treatments, the six most abundant bacteria at class levels were *Gammaproteobacteria* (an average relative abundance 55.11%), *Flavobacteriia* (9.43%), *Betaproteobacteria* (9.38%), followed by *Alphaproteobacteria* (8.79%), *Actinobacteria* (6.93%) and *Sphingobacteriia* (3.68%). The putative Hg methylators during the incubations water were *Clostridiaceae* (0.06–0.31%), *Ruminococcaceae* (0.01–0.06%), *unclassified Bacteria* (0.14–0.89%), *unclassified Deltaproteo bacteria* (0.00–0.02%), *unclassified Gammaproteobacteria* (0.00–0.20%), and *Enterobacteriaceae* (0.36–2.85%). As shown in Fig. S5, there was a positive correlation between *hgcA* gene and relative abundance of *Enterobacteriaceae* with a Pearson correlation coefficient of 0.94 ($P < 0.05$), indicating that

Enterobacteriaceae was likely a dominant methylator during the incubation.

Bacterial abundance is widely recognized as an important factor in the regulations of biotic Hg methylation and demethylation [11,32,43]. 16S rRNA gene abundance is considered an effective indicator for the total number of bacteria [49]. From the qPCR analyses, we observed significant increases in 16S rRNA gene abundance across the DOM treatments compared to the controls ($P < 0.05$) (Fig. 2d). Specifically, 16S rRNA gene abundance in AOM and TOM treatments were 752.99–2422.25 and 2.32–9.16 times higher than those in the control on day 7. However, the 16S rRNA gene abundance decreased in the AOM-A and AOM-E treatments, but increased in the TOM-S and TOM-W from day 7 to 14 (Fig. 2d).

During the incubation periods, *hgcA* gene abundance displayed similar trend as 16S rRNA gene abundance (Fig. 2e). On day 7, *hgcA* abundance in the AOM-A and AOM-E treatments was significantly higher than those in the TOM-S, TOM-W, and control treatments ($P < 0.05$). Furthermore, *hgcA* abundance in the AOM-A and AOM-E treatments steadily decreased from day 7 to day 14, which could be attributed to the consumption of labile carbon during incubation (see details in Section 3.4). The abundance of *merB* in the TOM treatment (i.e., 5.23×10^5–1.98×10^6 copies L^{-1}) was significantly higher than that in the control and AOM treatments during the incubations ($P < 0.05$). These investigations showed that DOM sources could play divergent roles in promoting methylation and demethylation in lake waters. The AOM treatments rapidly increased abundance of Hg methylators (compared to the control), whereas the TOM treatments increased the abundance of both Hg methylators and MeHg demethylators (Figs. 2e and 2f). In addition, the ratios of *hgcA*:16S rRNA gene in AOM treatments were predominantly higher than those in the controls and TOM treatments, indicating unique ability of AOM to stimulate Hg methylation (Fig. S6).

3.4. Characterization of different DOM composition during the incubation

As indicated in Fig. S7, the four original DOMs exhibited different characteristics in their EEM spectra. In general, the intensity of the tyrosine- or tryptophan-like fluorescence signature is stronger in AOM (Ex/Em: 230(280)/338), whereas the fluorescence region of TOM is mainly concentrated in the terrestrial humic-like compounds (Ex/Em: 265/460 and 355/432) [64]. The fluorescence intensities of the protein- and amino acid-like substance had decreased substantially in AOM treatments from day 0 to 14, whereas fluorescence intensities in the TOM and the control treatments remained stable (Fig. 3a and 3b). Fig. 3c illustrated the average alterations in fluorescence intensities across the five distinct groups. Notably, the API and APII, which are major components within AOM, exhibited a substantial decrease of 56.80 ± 18.72% and 44.42 ± 17.33%, respectively, during the period from day 0 to 14. This decrease underscores their highly labile nature during the incubation. In contrast, FA and HA only decreased by 26.09 ± 9.42%, and 19.32 ± 10.21%, respectively. DOM molecules were also detected using UPLC-QTOF-MS (Fig. S8). An increase in the number of the peaks corresponding to the hydrophilic substances (elution time < 5 min) and species with medium polarity (elution time between 5–15 min) was observed within the AOM groups, indicating that AOM contained highly abundant species (Fig. S9). In addition, the AOM groups showed higher and broader hydrophilic peaks at 1.3 and 1.8 min than the TOM groups, suggesting more hydrophilic components in the AOM. AOM-E had the lowest *m/z* ratio but the highest proportion of CHONS among the four sources of DOM (Fig. S10 and Table S4). The relative abundance of lipids, proteins, and unsaturated hydrocarbon compounds in the AOM treatments were 23.76–25.88%, 6.28–10.03%, and 8.08–12.15%, respectively, slightly higher than those in the TOM treatment (i.e., 23.03–23.21%, 5.77–6.00%, and 7.99–8.02%, respectively).

Thiol groups usually exhibit strong binding affinity for Hg and are widely recognized as crucial factors influencing Hg bioavailability. In our study, we observed that thiol concentration in AOM groups (2.01

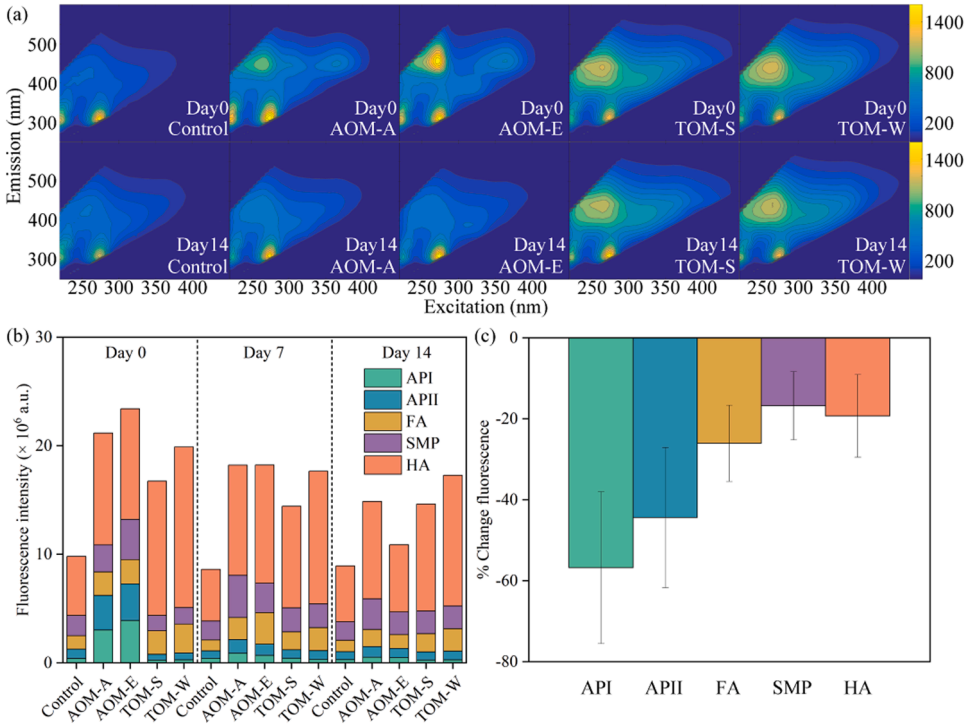

Fig. 3. Three dimensional fluorescence before and after the incubation (a), fluorescence intensity of FRI components in different samples during the incubation (b), and the changes of different components after 14 days (c); Aromatic Protein I (API), Aromatic Protein II (APII), Fluvic acid-like (FA), Soluble microbial by-product-like (SMP), Humic acid-like (HA).

± 0.18 μM for AOM-A and 2.41 ± 0.27 μM for AOM-E) were significantly higher ($P < 0.05$) than those in the TOM groups (0.80 ± 0.09 μM for TOM-S and 1.61 ± 0.13 μM for TOM-W) on day 0 (Fig. S11). Following the 14-day incubation, thiol concentrations increased in most of the groups, possibly due to the production and secretion of the thiol-containing compounds such as non-proteinaceous glutathione and phytochelatins [22].

In addition to the thiols, several other functional groups had exhibited changes during the incubation. A comparison of the FTIR spectra of different DOM samples had revealed distinct alterations (Fig. S12). The broad peak ranging from 3407 to 3422 cm^{-1} corresponds to O–H or N–H stretching, whereas the peak at 1642–1647 cm^{-1} signifies the C═O stretching of the amide groups. The peak at 1505 cm^{-1} was attributed to aromatic C═C vibrations, and the O–H peak at approximately 1420 cm^{-1} indicated the presence of carboxylic acids as major functional groups in the DOM samples. The C–O stretch peak at approximately 1140 cm^{-1} suggested the presence of polysaccharides like cellulose and lignin. During incubation, noteworthy increases in the peaks at 1642–1647, 1420, and 1140 cm^{-1} were observed in the AOM groups (Fig. S12b and c), indicating an increase in the corresponding functional groups and substances due to increased microbial metabolic activity. In contrast, the peaks of TOM at 1642–1647, 1505, and 1140 cm^{-1} exhibited greater intensity than those of AOM on day 0, suggesting that TOM had already undergone microbial transformations and degradations. Furthermore, peaks within the range of 650–994 cm^{-1} could be attributed to the C═C hydrogen bond or C–H out-of-plane vibrations.

4. Discussion

4.1. DOM compositions related to Hg methylation and MeHg demethylation processes

In the natural environments, the net production of MeHg is the result of both Hg methylation and MeHg demethylation processes [57,78]. DOM is recognized as one of the most essential factors in determining the biogeochemical cycling of Hg [44]. During the incubations, the average concentration of MeHg in the AOM treatment was 1.42 to 1.53 times higher than those in the TOM treatment and 1.65 to 1.79 times higher than that in the control (Fig. 2a). Notably, the AOM treatment enhanced the net MeHg production across all sampling intervals. Previous studies have implied that organic compounds derived from phytoplankton could stimulate the Hg methylation in the sediment of boreal lakes by increasing the overall bacterial activity [5]. Furthermore, the stable isotope tracers (Experiment 2) suggested that k_m in the AOM treatments was 1–2 orders of magnitude higher than those in the controls, whereas k_m was comparable in the TOM and control treatment (Fig. 2b).

Previous studies have suggested that low-molecular-weight organic thiols (e.g., cysteine and glutathione) promote the in situ Hg methylation [81]. In this study, UPLC-QTOF-MS results showed that AOM-E had the lowest m/z ratio and the highest proportion of CHONS substances (Table S4) among the four sources of DOM, indicating that AOM-E could be rapidly utilized by microbes, therefore promoting Hg methylation. However, the AOM-A treatment (the highest proportion of protein-like or unsaturated hydrocarbon-like substances) supply sufficient nutrients for the microbes and thus yielded the highest k_m value and net MeHg production during incubation. Lescord et al. [34] also revealed that MeHg concentrations in the lake and river waters are positively correlated with the amounts of microbial-based DOM or the proportions of labile and protein-like DOM, indicating the enhancements of Hg methylation. Moreover, the higher thiol concentrations in the AOM groups compared to the TOM groups may enhance the Hg (II)-ligand exchange between Hg(II)-thiol complexes and cell-associated proteins, thereby promoting Hg(II) uptakes and methylation [42]. The concentration of thiol ligands associated with DOM further influences the chemical speciation and bioavailability of MeHg, thereby controlling its bioaccumulations and biomagnification in aquatic food webs (Li et al., 2023; [62]). In addition, the DOM-induced changes in the k_d were stable within the same order of magnitude (i.e., 3.50–8.69 d^{-1}) regardless of the sources of DOM, indicating that AOM and TOM have quite different impacts on k_m and k_d.

4.2. Methylators and demethylators responded differently to DOM treatments

Herein, we found that the total number of bacteria (16S rRNA gene abundance) had increased under DOM treatments regardless of the sources, compared to the control treatments. The 16S rRNA gene abundance in the AOM treatment was substantially higher than that in the TOM treatment ($P < 0.05$; Fig. 2d). It shows that AOM is more readily metabolized by heterotrophs than TOM, indicating that AOM is more bioavailable to the heterotrophs than to TOM. It should be noted that both AOM or TOM could increase the abundance of *Deltaproteobacteria* carrying *hgcAB* genes. In addition, the *hgcA* gene abundance in the AOM treatments was significantly higher than that in the TOM treatment ($P < 0.05$). This observation is consistent with that of a recent study conducted in the eutrophic lake, in which the labile fraction of AOM was found to increase the abundance of potential Hg methylators, resulting in enhanced net MeHg production [33]. EEM spectra and UPLC-QTOF-MS analyses indicated that AOM contained more labile substances (e.g., lipids and proteins) than TOM, with major compositions of humic matter (Fig. 3b and S8). Abundant labile substances facilitated the growth of Hg methylators by stimulating microbial activities [5], increasing energy production [77] and providing methyl for methylation [51]. Besides, TOM yielded a higher abundance of *merB* than AOM (Fig. 2f), indicating that the influence of the DOM composition on Hg methylators and MeHg demethylators may be divergent.

Expanding on relationships between microbial abundance and methylation rates, we further investigated relations between specific DOM components, microbial community characteristics, and Hg methylation. Positive correlations were yielded between abundance of the 16S rRNA gene and *hgcA* gene vs. k_m values, with the Pearson correlation coefficients of 0.89 ($P < 0.05$) and 0.63 ($P < 0.05$), respectively. However, we failed to observe any correlation between k_d and the abundance of functional genes ($P > 0.05$, as Fig. S5). These investigations emphasize the significance of the overall microbial activity and exclusively Hg-methylating populations in predicting net MeHg formations. A significant positive relationship was observed between k_m and the intensity of specific DOM components (Fig. 4), including the API (R=0.52, $P < 0.05$), APII (R=0.52, $P < 0.05$), and SMP (R=0.48, $P < 0.1$). Thus, it is likely that DOM with a large abundance of amino acid and protein-like substances could primarily enhance methylation by stimulating bacterial activity. A previous study suggested that AOM components with the fewer aromatic, more oxygenated, and nitrogen-rich molecules at low molecular weights can serve as labile carbons for microbial methylator [33]. These components mainly correspond to the API, APII (e.g., tyrosine), and SMP (e.g., tryptophan phenylalanine, and tryptophan). In addition, no relationship between k_d and specific DOM components had been observed ($P > 0.1$), implying that k_d was less influenced by DOM during the incubation.

To identify the microbial taxa associated with Hg methylation and demethylation processes, a Mantel test was carried out using the data from 16S rRNA gene sequencing, qPCR gene copies, and the FRI components of the four DOMs (Fig. 5a). Regression analysis revealed significant positive correlations between the relative abundance of putative methylators and the API (R=0.42, $P < 0.05$), APII (R=0.62, $P < 0.01$), and SMP (R=0.55, $P < 0.01$) components, which was consistent with the observations of the DOM components and k_m (Fig. 4). A significant and positive correlation was also been observed between relative abundance of putative methylators and 16S rRNA gene copies (R=0.82,

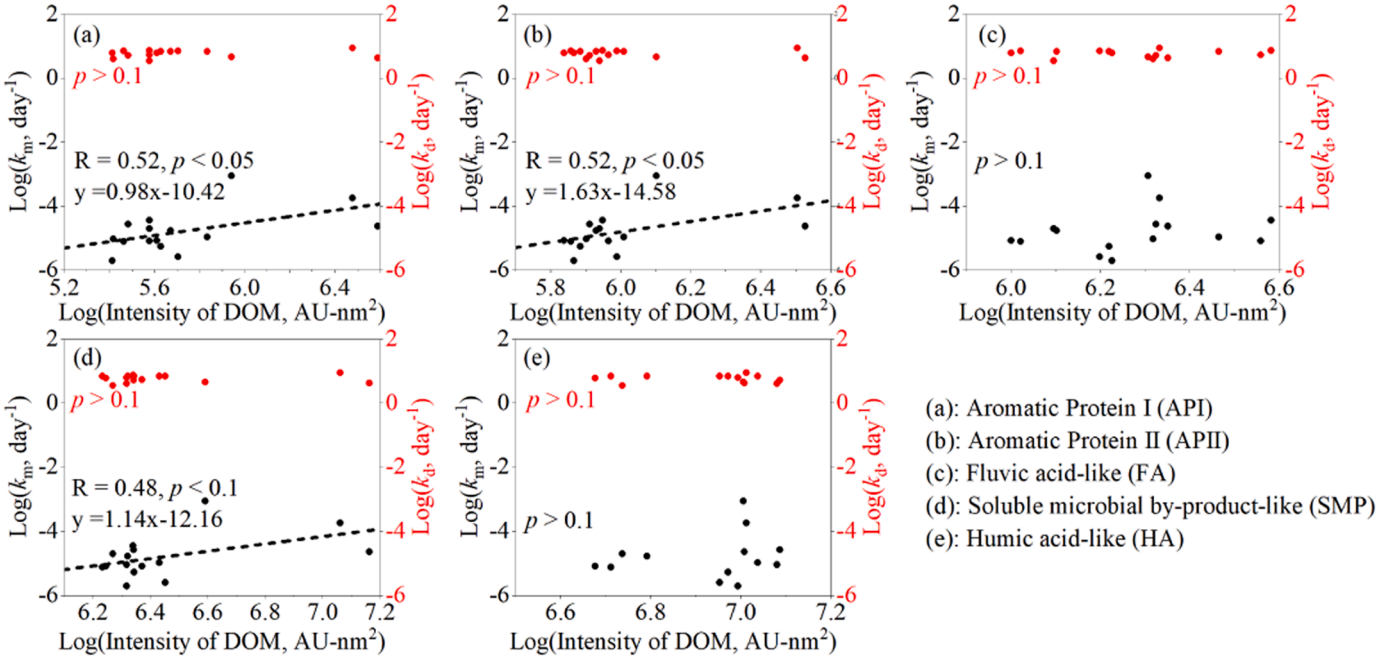

Fig. 4. Relationship between Hg methylation, MeHg demethylation rate constants and fluorescence intensities of the five DOM components (i.e., API, APII, FA, SMP, and HA); Aromatic Protein I (API), Aromatic Protein II (APII), Fluvic acid-like (FA), Soluble microbial by-product-like (SMP), Humic acid-like (HA).

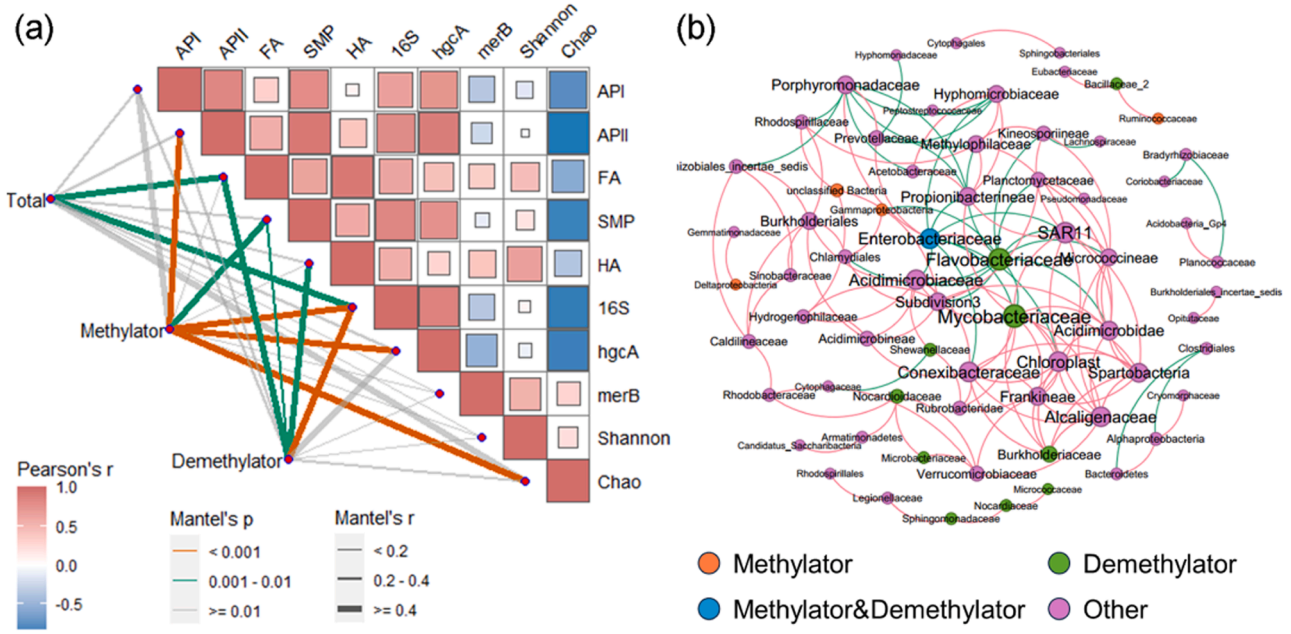

Fig. 5. Mantel test between the abundance of putative methylator and demethylators with the DOM composition, functional gene copies and alpha-diversity indexes (a). Networks showing the co-occurrence patterns among the putative methylators and demethylators (b). The edges connecting nodes indicate strong ($|\rho| > 0.5$) and significant ($p < 0.01$) correlations. Red edges show the positive correlations and green edges show the negative correlations.

$P < 0.01$), *hgcA* gene copies (R=0.81, $P < 0.01$), Chao index (R=0.76, $P < 0.01$). These findings suggested that the labile DOM components (i.e., API, APII, and SMP) play important roles in promoting Hg methylation in microbes. In contrast, the abundance of demethylators was positively correlated with HA (R=0.53, $P < 0.01$) and FA (R=0.40, $P < 0.01$) components in DOM, suggesting that DOM components have different effects on methylators and demethylators. We performed co-occurrence analyses to investigate the potential interaction between the putative methylators, demethylators, and other taxa based on strong correlations (correlation coefficient > 0.5, $P < 0.01$) (Fig. 5b). The results indicated that six putative methylators appeared in the correlation networks, and all exhibited positive correlations with non-methylators and non-demethylators. Notably, *Enterobacteriaceae* have been identified as the potential Hg methylators and MeHg demethylators [21,9], with strong correlations with various other taxa during the incubation. Similarly, *Enterobacteriaceae* and six other taxa were identified as connectors in the molecular ecological network analysis (Fig. S13) and were mainly responsible for the connection between modules [84]. Recently, Hao et al. [23] revealed that certain non-Hg methylator could promote the MeHg production through a syntrophic

relationship with Hg methylators. Regarding demethylation, *Flavobacteriaceae* and *Mycobacteriaceae* were strongly correlated with other taxa. Our results indicated that microbes without *hgcA* and *merB* in microbial communities could tightly associate with methylators or demethylators and therefore play significant roles in net MeHg productions. However, it should be noted that our findings were derived from microcosm experiments, and further investigation is required to extend our results to the field. We recognized that the correlations of microbial community and methylation/demethylation might only represent a statistical association rather than the direct evidences of causality. Metagenomic and transcriptomic analyses are necessary to provide more specific microbiological evidence for interactions between DOM and microbes.

5. Conclusion

Human activities have substantially altered the concentrations and compositions of DOM in lakes, which in turn influence the Hg cycling and risk in aquatic ecosystem. Our study suggested that risks and accumulation of MeHg in the aquatic ecosystem could be largely enhanced by the AOM input rather than the TOM input, as the former induces the increase in the abundance of methylators and methylation process. This result may be due to the presence of more labile amino acid and protein-like substances in the AOM which drive the entire microbial one-carbon metabolism process and stimulate growth of methylated microorganisms. Notably, our results showed that Hg methylators and MeHg demethylators respond differently to the DOM inputs, with abundance of Hg methylators changing more noticeably than that of MeHg demethylators under different DOM treatments. Furthermore, we observed that labile fractions of DOM (i.e., API, APII, and SMP) were correlated with enhancement of methylators and k_m value, indicating that these fractions could be used as effective indicator for predicting the net MeHg production in aquatic ecosystem. Our findings highlight divergent impacts of DOM from different sources on Hg methylation and MeHg demethylation due to different microbial responses, which should be considered in the Hg risk assessments in aquatic ecosystems.

CRediT authorship contribution statement

Pu Qiang: Methodology, Resources, Writing – review & editing. **Zhao Yingxin:** Resources. **He Wei:** Software, Visualization. **Liu Jiang:** Methodology, Resources, Writing – review & editing. **Liu Yurong:** Resources, Writing – review & editing. **Li Zhike:** Conceptualization, Methodology, Software, Validation. **Liu Yiwen:** Resources. **Wu Zhengyu:** Investigation, Methodology, Visualization, Writing – original draft, Writing – review & editing. **Meng Bo:** Funding acquisition, Methodology, Resources, Supervision, Writing – review & editing. **Wang Xuejun:** Resources. **Shao Bo:** Investigation, Resources, Software, Validation. **Tong Yindong:** Conceptualization, Funding acquisition, Methodology, Resources, Supervision, Writing – review & editing. **Cui Xiaomei:** Resources. **Chen Ji:** Investigation, Methodology, Resources, Writing – review & editing. **Liu Xianhua:** Resources. **Cui Xiaoyu:** Resources, Supervision, Visualization, Writing – review & editing.

Environmental Implication

The production of neurotoxic methylmercury (MeHg) is of global concern. The role of dissolved organic matter (DOM) in MeHg production is critical but not fully understood. This study used isotope tracers, RT-qPCR, and gene sequencing to investigate Hg methylation/demethylation processes and microbial responses to different DOM. Our results showed that DOM with distinct compositions affected methylators and demethylators differently. Labile fractions of DOM were correlated with methylators and methylation rate constants and may serve as indicators for predicting MeHg. These findings highlight the diverse influences of different DOM on methylation and demethylation, requiring consideration in Hg risk assessment.

Declaration of Competing Interest

The authors declare that they have no known competing financial interests or personal relationships that could have appeared to influence the work reported in this paper.

Data Availability

Data will be made available on request.

Acknowledgments

This study was funded by the National Natural Science Foundation, China (No. 42122059, 41977324 and 42377399) and Guizhou Provincial 2020 Science and Technology Subsidies (No. GZ2020SIG). We thanked Kun Zhang, Zhengdong Hao and Hongqian Yin, all from the Institute of Geochemistry, Chinese Academy of Sciences, for their help in MeHg isotope measurement.

Appendix A. Supporting information

Supplementary data associated with this article can be found in the online version at doi:10.1016/j.jhazmat.2023.133298.

References

[1] Aitken, A., Learmonth, M., 1996. Estimation of disulfide bonds using Ellman's reagent. In: Walker, J.M. (Ed.), The Protein Protocols Handbook. Humana Press, pp. 487–488.
[2] Bai, L., Cao, C., Wang, C., Xu, H., Zhang, H., Slaveykova, V.I., Jiang, H., 2017. Toward quantitative understanding of the bioavailability of dissolved organic matter in freshwater lake during cyanobacteria blooming. Environ Sci Technol 51 (11), 6018–6026.
[3] Barkay, T., Gu, B., 2021. Demethylation-the other side of the mercury methylation coin: a critical review. ACS Environ Au 2 (2), 77–97.
[4] Bravo, A.G., Cosio, C., 2019. Biotic formation of methylmercury: a bio-physico-chemical conundrum. Limnol Oceanogr 5 (65), 1010–1027.
[5] Bravo, A.G., Bouchet, S., Tolu, J., Björn, E., Mateos-Rivera, A., Bertilsson, S., 2017. Molecular composition of organic matter controls methylmercury formation in boreal lakes. Nat Commun 8 (1).
[6] Bravo, A.G., Kothawala, D.N., Attermeyer, K., Tessier, E., Bodmer, P., Ledesma, J.L. J., Audet, J., Casas-Ruiz, J.P., Catalán, N., Cauvy-Fraunié, S., Colls, M., Deininger, A., Evtimova, V.V., Fonvielle, J.A., Fuß, T., Gilbert, P., Herrero Ortega, S., Liu, L., Mendoza-Lera, C., Monteiro, J., Mor, J., Nagler, M., Niedrist, G. H., Nydahl, A.C., Pastor, A., Pegg, J., Gutmann Roberts, C., Pilotto, F., Portela, A.P., González-Quijano, C.R., Romero, F., Rulík, M., Amouroux, D., 2018. The interplay between total mercury, methylmercury and dissolved organic matter in fluvial systems: a latitudinal study across Europe. Water Res 144, 172–182.
[7] Catalán, N., Pastor, A., Borrego, C.M., Casas Ruiz, J.P., Hawkes, J.A., Gutiérrez, C., Schiller, D., Marcé, R., 2021. The relevance of environment vs. composition on dissolved organic matter degradation in freshwaters. Limnol Oceanogr 66 (2), 306–320.
[8] Chen, W., Westerhoff, P., Leenheer, J.A., Booksh, K., 2003. Fluorescence excitation-emission matrix regional integration to quantify spectra for dissolved organic matter. Environ Sci Technol 37 (24), 5701–5710.
[9] Christakis, C.A., Barkay, T., Boyd, E.S., 2021. Expanded diversity and phylogeny of mer genes broadens mercury resistance paradigms and reveals an origin for MerA among thermophilic archaea. Front Microbiol 12, 682605.
[10] Christensen, G.A., Wymore, A.M., King, A.J., Podar, M., Hurt, J.R.A., Santillan, E. U., Soren, A., Brandt, C.C., Brown, S.D., Palumbo, A.V., Wall, J.D., Gilmour, C.C., Elias, D.A., Oak Ridge National Lab. ORNL, O.R.T.U., Voordouw, G., 2016. Development and validation of broad-range qualitative and clade-specific quantitative molecular probes for assessing mercury methylation in the environment. In: Appl. Environ. Microbiol, 82, pp. 6068–6078.
[11] Christensen, G.A., Gionfriddo, C.M., King, A.J., Moberly, J.G., Miller, C.L., Somenahally, A.C., Callister, S.J., Brewer, H., Podar, M., Brown, S.D., Palumbo, A. V., Brandt, C.C., Wymore, A.M., Brooks, S.C., Hwang, C., Fields, M.W., Wall, J.D., Gilmour, C.C., Elias, D.A., 2019. Determining the reliability of measuring mercury cycling gene abundance with correlations with mercury and methylmercury concentrations. Environ Sci Technol 53 (15), 8649–8663.
[12] Daly, R.I., Ho, L., Brookes, J.D., 2007. Effect of chlorination on microcystis aeruginosa cell integrity and subsequent microcystin release and degradation. Environ Sci Technol 41 (12), 4447–4453.
[13] Deng, X., Ruan, L., Ren, R., Tao, M., Zhang, J., Wang, L., Yan, Y., Wen, X., Yang, X., Xie, P., 2022. Phosphorus accelerate the sulfur cycle by promoting the release of

malodorous volatile organic sulfur compounds from Microcystis in freshwater lakes. Sci Total Environ 845, 157280.
[14] Eckley, C.S., Luxton, T.P., Knightes, C.D., Shah, V., 2021. Methylmercury production and degradation under light and dark conditions in the water column of the hells Canyon Reservoirs, USA. Environ Toxicol Chem 40 (7), 1829–1839.
[15] Ellman, G.L., 1959. Tissue sulfhydryl groups. Arch Biochem Biophys 82, 70–77.
[16] Fleck, J.A., Gill, G., Bergamaschi, B.A., Kraus, T.E.C., Downing, B.D., Alpers, C.N., 2014. Concurrent photolytic degradation of aqueous methylmercury and dissolved organic matter. Sci Total Environ 484, 263–275.
[17] Fleming, E.J., Mack, E.E., Green, P.G., Nelson, D.C., 2006. Mercury methylation from unexpected sources: molybdate-inhibited freshwater sediments and an iron-reducing bacterium. Appl Environ Microbiol 72 (1), 457–464.
[18] Gascón Díez, E., Loizeau, J., Cosio, C., Bouchet, S., Adatte, T., Amouroux, D., Bravo, A.G., 2016. Role of settling particles on mercury methylation in the oxic water column of freshwater systems. Environ Sci Technol 50 (21), 11672–11679.
[19] Gilmour, C.C., Riedel, G.S., Ederington, M.C., Bell, J.T., Gill, G.A., Stordal, M.C., 1998. Methylmercury concentrations and production rates across a trophic gradient in the northern Everglades. Biogeochemistry 40 (2), 327–345.
[20] Gilmour, C.C., Elias, D.A., Kucken, A.M., Brown, S.D., Palumbo, A.V., Schadt, C.W., Wall, J.D., 2011. Sulfate-reducing bacterium desulfovibrio desulfuricans ND132 as a model for understanding bacterial mercury methylation. Appl Environ Microbiol 77 (12), 3938–3951.
[21] Gionfriddo, C.M., Wymore, A.M., Jones, D.S., Wilpiszeski, R.L., Lynes, M.M., Christensen, G.A., Soren, A., Gilmour, C.C., Podar, M., Elias, D.A., 2020. An Improved hgcAB primer set and direct high-throughput sequencing expand Hg-methylator diversity in nature. Front Microbiol 11, 541554.
[22] Guimarães-Soares, L., Pascoal, C., Cássio, F., 2007. Effects of heavy metals on the production of thiol compounds by the aquatic fungi Fontanospora fusiramosa and Flagellospora curta. Ecotox Environ Safe 66 (1), 36–43.
[23] Hao, Y., Liu, H., Zhao, J., Feng, J., Hao, X., Huang, Q., Gu, B., Liu, Y., 2023. Plastispheres as hotspots of microbially-driven methylmercury production in paddy soils. J Hazard Mater 457, 131699.
[24] Harris, R.C., Rudd, J.W., Amyot, M., Babiarz, C.L., Beaty, K.G., Blanchfield, P.J., Bodaly, R.A., Branfireun, B.A., Gilmour, C.C., Graydon, J.A., Heyes, A., Hintelmann, H., Hurley, J.P., Kelly, C.A., Krabbenhoft, D.P., Lindberg, S.E., Mason, R.P., Paterson, M.J., Podemski, C.L., Robinson, A., Sandilands, K.A., Southworth, G.R., St, L.V., Tate, M.T., 2007. Whole-ecosystem study shows rapid fish-mercury response to changes in mercury deposition. Proc Natl Acad Sci Usa 104 (42), 16586–16591.
[25] He, W., Chen, M., Park, J., Hur, J., 2016. Molecular diversity of riverine alkaline-extractable sediment organic matter and its linkages with spectral indicators and molecular size distributions. Water Res 100, 222–231.
[26] Hintelmann, H., Keppel-Jones, K., Evans, R.D., 2000. Constants of mercury methylation and demethylation rates in sediments and comparison of tracer and ambient mercury availability. Environ Toxicol Chem 19 (9), 2204–2211.
[27] Hsu-Kim, H., Eckley, C.S., Achá, D., Feng, X., Gilmour, C.C., Jonsson, S., Mitchell, C.P.J., 2018. Challenges and opportunities for managing aquatic mercury pollution in altered landscapes. Ambio 47 (2), 141–169.
[28] Jiang, T., Kaal, J., Liang, J., Zhang, Y., Wei, S., Wang, D., Green, N.W., 2017. Composition of dissolved organic matter (DOM) from periodically submerged soils in the Three Gorges Reservoir areas as determined by elemental and optical analysis, infrared spectroscopy, pyrolysis-GC-MS and thermally assisted hydrolysis and methylation. Sci Total Environ 603-604, 461–471.
[29] Jiang, T., Bravo, A.G., Skyllberg, U., Björn, E., Wang, D., Yan, H., Green, N.W., 2018. Influence of dissolved organic matter (DOM) characteristics on dissolved mercury (Hg) species composition in sediment porewater of lakes from southwest China. Water Res 146, 146–158.
[30] Koch, B.P., Dittmar, T., 2006. From mass to structure: an aromaticity index for high-resolution mass data of natural organic matter. Rapid Commun Mass Spectrom 20 (5), 926–932.
[31] Kowalczuk, P., Tilstone, G.H., Zabłocka, M., Röttgers, R., Thomas, R., 2013. Composition of dissolved organic matter along an Atlantic meridional transect from fluorescence spectroscopy and parallel factor analysis. Mar Chem 157, 170–184.
[32] Lei, P., Nunes, L.M., Liu, Y., Zhong, H., Pan, K., 2019. Mechanisms of algal biomass input enhanced microbial Hg methylation in lake sediments. Environ Int 126, 279–288.
[33] Lei, P., Zhang, J., Zhu, J., Tan, Q., Kwong, R.W.M., Pan, K., Jiang, T., Naderi, M., Zhong, H., 2021. Algal organic matter drives methanogen-mediated methylmercury production in water from eutrophic shallow lakes. Environ Sci Technol 55 (15), 10811–10820.
[34] Lescord, G.L., Emilson, E.J.S., Johnston, T.A., Branfireun, B.A., Gunn, J.M., 2018. Optical properties of dissolved organic matter and their relation to mercury concentrations in water and biota across a remote freshwater drainage basin. Environ Sci Technol 52 (6), 3344–3353.
[35] Li, Y., Li, D., Song, B., Li, Y., 2022. The potential of mercury methylation and demethylation by 15 species of marine microalgae. Water Res 215, 118266.
[36] Li, Z., Wu, Z., Shao, B., Tanentzap, A.J., Chi, J., He, W., et al., 2023. Biodegradability of algal-derived dissolved organic matter and its influence on methylmercury uptake by phytoplankton. Water Res 242, 120175.
[37] Li, Z., Chi, J., Shao, B., Wu, Z., He, W., Liu, Y., Sun, P., Lin, H., Wang, X., Zhao, Y., Chen, L., Tong, Y., 2022. Inhibition of methylmercury uptake by freshwater phytoplankton in presence of algae-derived organic matter. Environ Pollut 313, 120111.
[38] Liu, J., Meng, B., Poulain, A.J., Meng, Q., Feng, X., 2021. Stable isotope tracers identify sources and transformations of mercury in rice (Oryza sativa L.) growing in a mercury mining area. Fundam Res 1 (3), 259–268.
[39] Liu, J., Lu, B., Poulain, A.J., Zhang, R., Zhang, T., Feng, X., Meng, B., 2022. The underappreciated role of natural organic matter bond Hg(II) and nanoparticulate HgS as substrates for methylation in paddy soils across a Hg concentration gradient. Environ Pollut 292, 118321.
[40] Liu, J., Chen, J., Poulain, A.J., Pu, Q., Hao, Z., Meng, B., Feng, X., 2023. Mercury and sulfur redox cycling affect methylmercury levels in rice paddy soils across a contamination gradient. Environ Sci Technol 57 (21), 8149–8160.
[41] Liu, J., Li, Y., Duan, D., Peng, G., Li, P., Lei, P., Zhong, H., Tsui, M.T., Pan, K., 2022. Effects and mechanisms of organic matter regulating the methylmercury dynamics in mangrove sediments. J Hazard Mater 432, 128690.
[42] Liu, Y., Lu, X., Zhao, L., An, J., He, J., Pierce, E., Johs, A., Gu, B., 2016. Effects of cellular sorption on mercury bioavailability and methylmercury production by Desulfovibrio desulfuricans ND132. Environ Sci Technol 50 (24), 13335–13341.
[43] Liu, Y., Johs, A., Bi, L., Lu, X., Hu, H., Sun, D., He, J., Gu, B., 2018. Unraveling microbial communities associated with methylmercury production in paddy soils. Environ Sci Technol 52 (22), 13110–13118.
[44] Ma, M., Du, H., Wang, D., 2019. Mercury methylation by anaerobic microorganisms: a review. Crit Rev Environ Sci Technol 20 (49), 1893–1936.
[45] Mazrui, N.M., Jonsson, S., Thota, S., Zhao, J., Mason, R.P., 2016. Enhanced availability of mercury bound to dissolved organic matter for methylation in marine sediments. Geochim Cosmochim Acta 194, 153–162.
[46] Meng, B., Feng, X., Qiu, G., Liang, P., Li, P., Chen, C., Shang, L., 2011. The process of methylmercury accumulation in rice (Oryza sativa L.). Environ Sci Technol 45 (7), 2711–2717.
[47] Merritt, K.A., Amirbahman, A., 2009. Mercury methylation dynamics in estuarine and coastal marine environments-a critical review. Earth-Sci Rev 96 (1-2), 54–66.
[48] Noh, S., Kim, J., Hur, J., Hong, Y., Han, S., 2018. Potential contributions of dissolved organic matter to monomethylmercury distributions in temperate reservoirs as revealed by fluorescence spectroscopy. Environ Sci Pollut Res 25 (7), 6474–6486.
[49] Oyarzúa, P., Bovio-Winkler, P., Etchebehere, C., Suárez-Ojeda, M.E., 2021. Microbial communities in an anammox reactor treating municipal wastewater at mainstream conditions: practical implications of different molecular approaches. J Environ Chem Eng 9 (6), 106622.
[50] Packer, B.N., Carling, G.T., Veverica, T.J., Russell, K.A., Nelson, S.T., Aanderud, Z. T., 2020. Mercury and dissolved organic matter dynamics during snowmelt runoff in a montane watershed, Provo River, Utah, USA. Sci Total Environ 704, 135297.
[51] Paranjape, A.R., Hall, B.D., 2017. Recent advances in the study of mercury methylation in aquatic systems. Facets 2 (1), 85–119.
[52] Parks, J.M., Johs, A., Podar, M., Bridou, R., Hurt, R.A., Smith, S.D., Tomanicek, S. J., Qian, Y., Brown, S.D., Brandt, C.C., Palumbo, A.V., Smith, J.C., Wall, J.D., Elias, D.A., Liang, L., 2013. The genetic basis for bacterial mercury methylation. Science 339 (6125), 1332–1335.
[53] Patriarca, C., Sedano-Núñez, V.T., Garcia, S.L., Bergquist, J., Bertilsson, S., Sjöberg, P.J.R., et al., 2021. Character and environmental lability of cyanobacteria-derived dissolved organic matter. Limnol Oceanogr 66, 496–509.
[54] Poste, A.E., Hoel, C.S., Andersen, T., Arts, M.T., Færøvig, P., Borgå, K., 2019. Terrestrial organic matter increases zooplankton methylmercury accumulation in a brown-water boreal lake. Sci Total Environ 674, 9–18.
[55] Qin, F., Amyot, M., Bertolo, A., 2023. The relationship between zooplankton vertical distribution and the concentration of aqueous Hg in boreal lakes: A comparative field study. Sci Total Environ 858, 159793.
[56] R Core Team, A., 2017. R: A language and environment for statistical computing, Vienna, Austria.
[57] Regnell, O., Watras, C.J., 2018. Microbial mercury methylation in aquatic environments: a critical review of published field and laboratory studies. Environ Sci Technol 53 (1), 4–19.
[58] Rodríguez Martín-Doimeadios, R.C., Krupp, E., Amouroux, D., Donard, O.F.X., 2002. Application of isotopically labeled methylmercury for isotope dilution analysis of biological samples using gas chromatography/ICPMS. Anal Chem 74 (11), 2505–2512.
[59] Schaefer, J.K., Morel, F.M.M., 2009. High methylation rates of mercury bound to cysteine by Geobacter sulfurreducens. Nat Geosci 2 (2), 123–126.
[60] Schaefer, J.K., Yagi, J., Reinfelder, J.R., Cardona, T., Ellickson, K.M., Tel-Or, S., Barkay, T., 2004. Role of the bacterial organomercury lyase (MerB) in controlling methylmercury accumulation in mercury-contaminated natural waters. Environ Sci Technol 38 (16), 4304–4311.
[61] Schartup, A.T., Mason, R.P., Balcom, P.H., Hollweg, T.A., Chen, C.Y., 2012. Methylmercury production in estuarine sediments: role of organic matter. Environ Sci Technol 47 (2), 695–700.
[62] Seelen, E., Liem-Nguyen, V., Wünsch, U., Baumann, Z., Mason, R., Skyllberg, U., Björn, E., 2023. Dissolved organic matter thiol concentrations determine methylmercury bioavailability across the terrestrial-marine aquatic continuum. Nat Commun 14 (1), 6728.
[63] Shahmohamadloo, R.S., Ortiz Almirall, X., Simmons, D.B.D., Lumsden, J.S., Bhavsar, S.P., Watson-Leung, T., Eyken, A.V., Hankins, G., Hubbs, K., Konopelko, P., Sarnacki, M., Strong, D., Sibley, P.K., 2021. Cyanotoxins within and outside ofmicrocystis aeruginosa cause adverse effects in rainbow trout (Oncorhynchus mykiss). Environ Sci Technol 55 (15), 10422–10431.
[64] Shi, W., Zhuang, W., Hur, J., Yang, L., 2021. Monitoring dissolved organic matter in wastewater and drinking water treatments using spectroscopic analysis and ultra-high resolution mass spectrometry. Water Res 188, 116406.

[65] Sinclair, L., Osman, O.A., Bertilsson, S., Eiler, A., 2015. Microbial community composition and diversity via 16S rRNA gene amplicons: evaluating the illumina platform. Plos One 10 (2), e116955.
[66] Stedmon, C.A., Bro, R., 2008. Characterizing dissolved organic matter fluorescence with paral- lel factor analysis: a tutorial. Limnol Oceano: Methods 6, 1–6.
[67] Stein, E.D., Cohen, Y., Winer, A.M., 1996. Environmental distribution and transformation of mercury compounds. Crit Rev Environ Sci Technol 26 (1), 1–43.
[68] Tong, Y., Wang, M., Bu, X., Guo, X., Lin, Y., Lin, H., Li, J., Zhang, W., Wang, X., 2017. Mercury concentrations in China's coastal waters and implications for fish consumption by vulnerable populations. Environ Pollut 231, 396–405.
[69] Ullrich, S.M., Tanton, T.W., Abdrashitova, S.A., 2001. Mercury in the aquatic environment; a review of factors affecting methylation. Crit Rev Environ Sci Technol 31 (3), 241–293.
[70] Wang, B., Hu, H., Bishop, K., Buck, M., Björn, E., Skyllberg, U., Nilsson, M.B., Bertilsson, S., Bravo, A.G., 2023. Microbial communities mediating net methylmercury formation along a trophic gradient in a peatland chronosequence. J Hazard Mater 442, 130057.
[71] Wang, S., Zhang, M., Li, B., Xing, D., Wang, X., Wei, C., Jia, Y., 2012. Comparison of mercury speciation and distribution in the water column and sediments between the algal type zone and the macrophytic type zone in a hypereutrophic lake (Dianchi Lake) in Southwestern China. Sci Total Environ 417-418, 204–213.
[72] Wang, T., Yang, X., Li, Z., Chen, W., Wen, X., He, Y., Ma, C., Yang, Z., Zhang, C., 2023. MeHg production in eutrophic lakes: focusing on the roles of algal organic matter and iron-sulfur-phosphorus dynamics. J Hazard Mater 457, 131682.
[73] Wu, Q., Hu, H., Meng, B., Wang, B., Poulain, A.J., Zhang, H., Liu, J., Bravo, A.G., Bishop, K., Bertilsson, S., Feng, X., 2020. Methanogenesis is an important process in controlling MeHg concentration in rice paddy soils affected by mining activities. Environ Sci Technol 54 (21), 13517–13526.
[74] Yan, H., Li, Q., Meng, B., Wang, C., Feng, X., He, T., Dominik, J., 2013. Spatial distribution and methylation of mercury in a eutrophic reservoir heavily contaminated by mercury in Southwest China. Appl Geochem 33, 182–190.
[75] Yin, X., Wang, L., Liang, X., Zhang, L., Zhao, J., Gu, B., 2022. Contrary effects of phytoplankton chlorella vulgaris and its exudates on mercury methylation by iron- and sulfate-reducing bacteria. J Hazard Mater 433, 128835.
[76] Yu, R., Reinfelder, J.R., Hines, M.E., Barkay, T., 2013. Mercury methylation by the methanogen methanospirillum hungatei. Appl Environ Microbiol 79 (20), 6325–6330.
[77] Yu, R., Reinfelder, J.R., Hines, M.E., Barkay, T., 2018. Syntrophic pathways for microbial mercury methylation. Isme J 12 (7), 1826–1835.
[78] Yu, R.Q., Barkay, T., 2022. Microbial mercury transformations: molecules, functions and organisms. Adv Appl Microbiol 118, 31–90.
[79] Zeng, L., McGowan, S., Swann, G.E.A., Leng, M.J., Chen, X., 2022. Eutrophication has a greater influence on floodplain lake carbon cycling than dam installation across the middle Yangtze region. J Hydrol 614, 128510.
[80] Zhao, J.Y., Ye, Z.H., Zhong, H., 2018. Rice root exudates affect microbial methylmercury production in paddy soils. Environ Pollut 242, 1921–1929.
[81] Zhao, L., Chen, H., Lu, X., Lin, H., Christensen, G.A., Pierce, E.M., Gu, B., 2017. Contrasting effects of dissolved organic matter on mercury methylation by geobacter sulfurreducens PCA andDesulfovibrio desulfuricans ND132. Environ Sci Technol 51 (18), 10468–10475.
[82] Zhou, Y., Davidson, T.A., Yao, X., Zhang, Y., Jeppesen, E., de Souza, J.G., Wu, H., Shi, K., Qin, B., 2018. How autochthonous dissolved organic matter responds to eutrophication and climate warming: evidence from a cross-continental data analysis and experiments. Earth-Sci Rev 185, 928–937.
[83] Zhou, Y., Zhou, L., Zhang, Y., Zhu, G., Qin, B., Jang, K., Spencer, R.G.M., Kothawala, D.N., Jeppesen, E., Brookes, J.D., Wu, F., 2022. Unraveling the role of anthropogenic and natural drivers in shaping the molecular composition and bioavailability of dissolved organic matter in non-pristine lakes. Environ Sci Technol 56 (7), 4655–4664.
[84] Zhu, M., Jing, Z., Zheng, Q., Du, S., Ya, T., Wang, X., 2020. Microbial network succession along a current gradient in a bio-electrochemical system. Bioresour Technol 314, 123741.